Available online at www.sciencedirect.com
SCIENCE DIRECT®
International Journal of Heat and Mass Transfer 48 (2005) 5386–5394
International Journal of HEAT and MASS TRANSFER
www.elsevier.com/locate/ijhmt

Thermal performance measurement of heat sinks with confined impinging jet by infrared thermography

Hung-Yi Li [a,*], Shung-Ming Chao [a], Go-Long Tsai [b]

[a] Department of Mechatronic Engineering, Huafan University, Shihtin, Taipei 22305, Taiwan, ROC
[b] Department of Vehicle Engineering, National Taipei University of Technology, Taipei 10626, Taiwan, ROC

Received 2 March 2005; received in revised form 1 July 2005
Available online 1 September 2005

Abstract

In this paper, the thermal performance of heat sinks with confined impingement cooling is measured by infrared thermography. The effects of the impinging Reynolds number, the width and the height of the fins, the distance between the nozzle and the tip of the fins, and the type of the heat sinks on the thermal resistance are investigated. The results show that increasing the Reynolds number of the impinging jet reduces the thermal resistance of the heat sinks consistently. However, the reduction of the thermal resistance decreases gradually with the increase of the Reynolds number. The thermal resistance can be decreased by increasing the fin width combined with an appropriate Reynolds number. Increasing the fin height to enlarge the area of heat transfer also decreases the thermal resistance, but the effects are less conspicuous than those on altering the fin width. An appropriate impinging distance with minimum thermal resistance can be found at a specific Reynolds number, and the optimal impinging distance increases as the Reynolds number increases. Generally speaking, the thermal performance of the pin–fin heat sinks is superior to that of the plate–fin heat sinks because the pin–fin heat sinks consist of smaller volumes but greater exposure surfaces.

Keywords: Confined impingement jet; Pin–fin heat sink; Plate–fin heat sink; Infrared thermography

1. Introduction

The cooling performance of electronic devices has attracted increasing attention owing to the demands of compact size and powerful computing ability. Although the technology of cooling has greatly advanced, the main cause of malfunction of the electronic devices remains because of local overheating. The problem arises from the restriction of a confined space. For a global consideration of setup in electronic equipment, flow recirculation and separation might result in poor transport of dissipated heat due to failure of effective convective flow. To overcome the overheating problem in electronic cooling, the understanding of fluid motion and heat transfer should hence achieve a greater depth. The heat transfer of heat sinks with an impinging jet in a confined space shows direct, quick and local cooling characteristics; this approach is generally applicable for cooling of electronic devices. The objective of our work has been to examine the

* Corresponding author. Tel.: +886 2 26632102x4017; fax: +886 2 26632102x4013.
E-mail address: hyli@huafan.hfu.edu.tw (H.-Y. Li).

0017-9310/$ - see front matter © 2005 Elsevier Ltd. All rights reserved.
doi:10.1016/j.ijheatmasstransfer.2005.07.007

Nomenclature

A	cross-sectional area of the heating element (mm^2)
A_t	heat transfer area (mm^2)
b	thickness of the base of the heat sink (mm)
D	diameter of the nozzle (mm)
d	distance between the two thermocouples in the heating element (mm)
G	inter-fin spacing (mm)
H	height of the fins (mm)
k_{al}	thermal conductivity of aluminum alloy (W/mK)
L	length of the base of the heat sink (mm)
n	fin number
Q	heating power (W)
Re	Reynolds number
R_{th}	thermal resistance (°C/W)
T	temperature (°C)
T_{ave}	mean temperature of the heat sink (°C)
T_l	temperature of the lower thermocouple in the heating element (°C)
T_u	temperature of the upper thermocouple in the heating element (°C)
T_∞	temperature of the impinging jet (°C)
U	overall heat transfer coefficient ($W/°C\ mm^2$)
V	jet velocity (m/s)
V_t	total volume of the heat sink (mm^3)
W	width of the fins (mm)
Y	distance between the nozzle and the tip of the fins (mm)

Greek symbol

v	kinematic viscosity (m^2/s)

influence of the velocity of an impinging jet, the impinging distance, the geometric shape and dimensions of heat sinks on the thermal performance under the condition of a confined space. Many experimental data were collected for this reason.

Yu and Joshi [1] studied combined natural convection, conduction, and radiation heat transfer of a pin–fin heat sink in a confined space through both experimental measurement and numerical simulation; they concluded that the confined space plays an important role in the heat transfer from the heat sink, and thermal radiation contributes significantly to the heat transfer. Sathe et al. [2] investigated the fluid motion and heat transfer from a heat sink under an impinging flow; their simulations and experiments of the local temperatures showed similar results for the central part of the heat sink, but simulations overpredicted the temperatures around the outer edge of the heat sink base. Teuscher et al. [3] used an impinging liquid to investigate heat transfer on both pin–fin and plate–fin heat sinks in confined spaces; their results showed that both pin–fin and plate–fin heat sinks yield heat transfer evidently increased over that from a smooth surface with the same base area. Experiments of Brignoni and Garimella [4] focused on the heat transfer of a confined jet flow impinging on a pin–fin heat sink; with a fixed nozzle-to-target spacing, these workers varied the flow speed, diameter of nozzle and nozzle arrays and found that at a fixed air flow rate a nozzle of smaller diameter increased the impinging velocity and decreased the thermal resistance. Ledezma et al. [5] were concerned with the optimization of the heat transfer from pin–fins under impinging air flow; they expressed the correlations for optimal fin-to-fin spacing and maximum thermal conductance. Maveety and Jung [6] investigated the cooling performance of a pin–fin heat sink with air impingement flow; their simulations demonstrated a complicated fluid motion inside the fins and a greater pressure gradient improved mixing and heat transfer. They concluded also that the heat transfer was greatly affected by the fin dimensions.

The infrared thermal imaging method utilizes the radiant existence in the infrared spectral band from measured objects to measure temperature. It is non-intrusive, applicable remotely and suitable for measurement of a large area, and can also serve to record data for subsequent storage and processing with a computer. Meinders et al. [7] applied both infrared thermography and liquid crystal thermography to investigate local convective heat transfer from cubes in tunnel flow; these methods exhibited satisfactory consistency. Meinders and Hanjalić [8] investigated the heat transfer coefficient of an array of cubic objects in turbulent tunnel flow by measuring the surface temperature with infrared thermography; they also used Laser Doppler Anemometry to measure the velocity distribution. Ay et al. [9] used an infrared thermal imaging camera to observe the surface temperature of a plate–finned-tube heat exchanger and calculated the local heat transfer coefficient.

In this paper, we focus on the interaction of confined jet flow impinging on both pin–fin heat sinks and plate–fin heat sinks using infrared thermography. The effects of the impinging Reynolds number, the width and the height of the fins, the distance between the nozzle and the tip of the fins, and the type of the heat sinks on the thermal performance are discussed.

2. Experimental apparatus and data reduction

The equipment for our experiments consists of an infrared thermal imaging system, a confined impinging jet system, heat sinks, a heating element and thermal isolation device, and a system to measure flow rate and temperature. A schematic diagram appears in Fig. 1.

The infrared thermal imaging system (FLIR systems' ThermaCAM SC500 camera and AGEMA Research software) has a range of temperature measurement from −20 °C to 1500 °C with ±2% accuracy. The IR camera utilizes a 320×240 pixels uncooled focal plane array detector operated over the wavelength range from 7.5 μm to 13 μm. The field of view is $24° \times 18°$, the instantaneous field of view is 1.3 mrad, and the thermal sensitivity is 0.1 °C at 30 °C. Images is transferred to a computer in almost real time and stored therein for further analysis.

The confined impinging jet system consists of a converging nozzle, orifice meters and a blower. A confining plate around the edge of the nozzle exit serves to confine the impinging jet. The base of the heat sink is also confined with an extension plate attached on the sides. The fluid temperature of the jet is measured with a thermocouple embedded in the nozzle. A nozzle of diameter (D) 8 mm is used and the distance (Y) between the nozzle and the tip of the fins is set as 96 mm for reference.

The heat sinks tested are distinguished by their two geometries, namely a pin–fin heat sink and a plate–fin heat sink of the same material, aluminium alloy 6061. To increase the accuracy of temperature measurement, all surfaces of heat sinks are coated with a flat black paint that has a radiation emissivity of 0.96. The pin–fin heat sink model is designed as an array of 6×6, whereas the plate–fin heat sink model is 6×2 with a cut-off passage in the x-direction. The bases of both models have the same length and width ($L = 80$ mm), and the thickness (b) of the bases is 8 mm. The length and width of the fins are varied as experimental parameters. We test 14 heat sinks, nine for the pin–fin heat sink model and five for the plate–fin heat sink model. The widths (W) are 6.5, 8.0 and 9.5 mm, whereas the heights (H) are 35, 40 and 45 mm, respectively. The denotations and dimensions are depicted in Table 1 and Figs. 2 and 3, respectively. The heat transfer areas of the pin–fin heat sink and the plate–fin heat sink are give by $A_t = L^2 + 4nWH$ and $A_t = L^2 + nH(2W + L - G)$, respectively. The total volumes of the pin–fin heat sink and the plate–fin heat sink are give by $V_t = L^2 b + nW^2 H$ and $V_t = L^2 b + nWH(L - G)/2$, respectively.

The heating element is covered with the insulated material, except on the top where it is in contact with the heat sink. The heating power is supplied from a DC source. It is expressed as

$$Q = \frac{k_{al} A (T_l - T_u)}{d} \tag{1}$$

in which k_{al} denotes the thermal conductivity of heating aluminum alloy 6061 and has a value 168 W/mK. T_u and T_l are the temperatures of the upper and lower thermocouples, respectively, installed in the heating element. A signifies the cross-sectional area of the heating

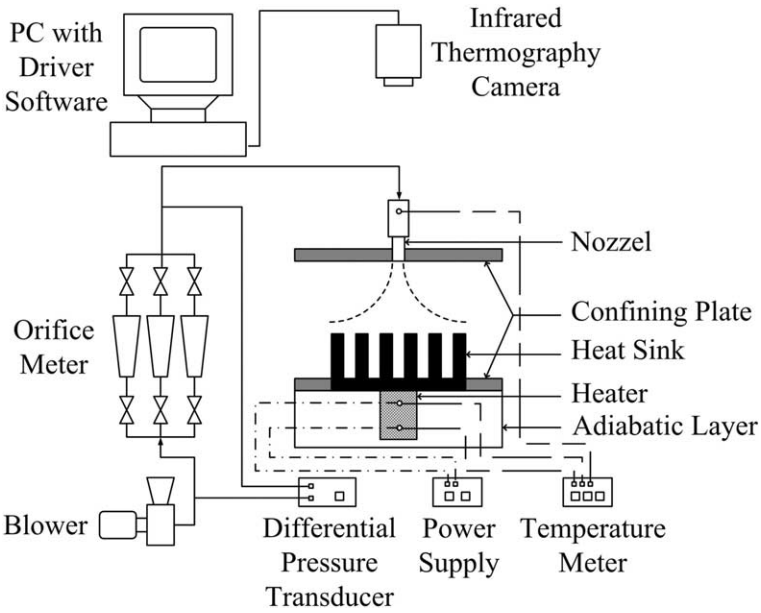

Fig. 1. The schematic diagram of the experimental apparatus.

Table 1
The specifications of the heat sinks

No.	Fin type	W (mm)	G (mm)	H (mm)	A_t (mm^2)	V_t (mm^3)
1	Pin–fin	6.5($W/L = 0.08125$)	8.2($G/L = 0.1025$)	35($H/L = 0.4375$)	39,160	10,4435
2				40($H/L = 0.5000$)	43,840	112,040
3				45($H/L = 0.5625$)	48,520	119,645
4		8.0($W/L = 0.10000$)	6.4($G/L = 0.0800$)	35($H/L = 0.4375$)	46,720	13,1840
5				40($H/L = 0.5000$)	52,480	143,360
6				45($H/L = 0.5625$)	58,240	154,880
7		9.5($W/L = 0.11875$)	4.6($G/L = 0.0575$)	35($H/L = 0.4375$)	54,280	164,915
8				40($H/L = 0.5000$)	61,120	181,160
9				45($H/L = 0.5625$)	67,960	197,405
10	Plate–fin	6.5($W/L = 0.08125$)	8.2($G/L = 0.1025$)	40($H/L = 0.5000$)	47,104	163,208
11		8.0($W/L = 0.10000$)	6.4($G/L = 0.0800$)	35($H/L = 0.4375$)	44,032	174,848
12				40($H/L = 0.5000$)	49,408	192,512
13				45($H/L = 0.5625$)	54,784	210,176
14		9.5($W/L = 0.11875$)	4.6($G/L = 0.0575$)	40($H/L = 0.5000$)	51,712	223,112

$L = 80$ mm, $b = 8$ mm

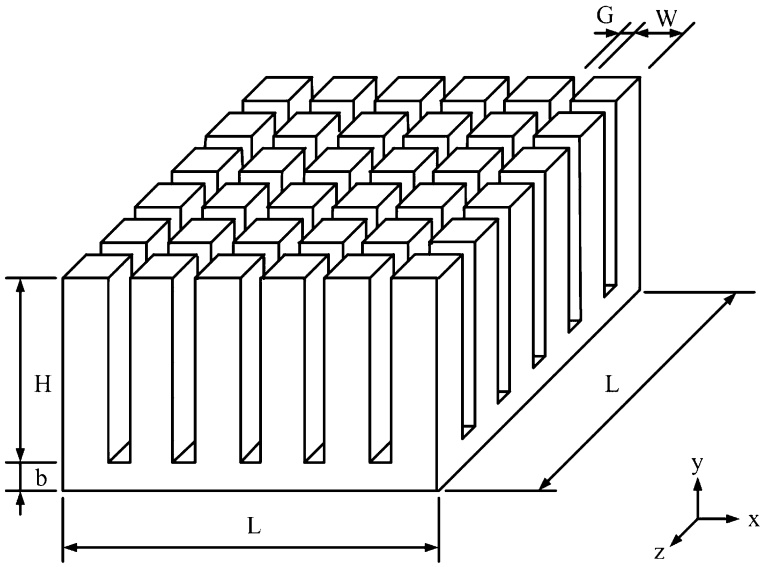

Fig. 2. The sketch of a pin–fin heat sink.

element, and d denotes the distance between the upper and lower thermocouples. The range of heating power in the experiments is 19.43–21.81 W. From our investigation of the influence of varying the heating power we conclude that it does not alter the thermal resistances over the range examined [10].

We use three orifice meters to cover the range of measurements 0.039–0.099 m^3/min, 0.059–0.189 m^3/min and 0.133–0.283 m^3/min. T-type thermocouples are used to measure temperatures of both the jet fluid and the heating element.

The experiments are performed and the temperature distributions obtained by the infrared thermal imaging system are manipulated with a computer and associated software. We thereby obtain the mean surface temperature of the heat sink and evaluate the thermal performance.

The thermal resistance is defined as

$$R_{th} = \frac{T_{ave} - T_\infty}{Q} = \frac{1}{UA_t} \tag{2}$$

where T_{ave} is the average temperature of the heat sink, T_∞ is the temperature of the impinging jet, U is the overall heat transfer coefficient, and A_t is the heat transfer area which consists of the top of the base and the fins of the heat sink. A smaller thermal resistance present

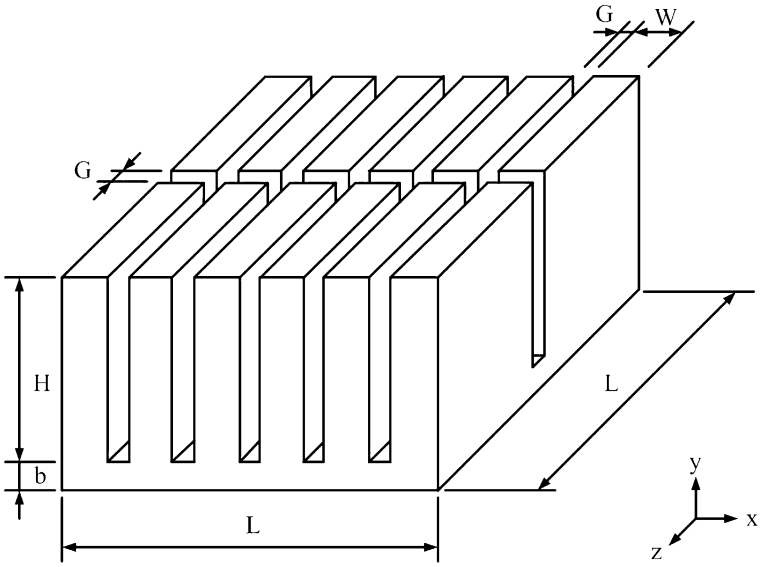

Fig. 3. The sketch of a plate–fin heat sink.

in the heat sink means that greater thermal energy is carried away for the same temperature difference, so with increased thermal performance. The Reynolds number of the impinging jet is calculated by

$$Re = \frac{VD}{v} \tag{3}$$

where V is the velocity and v is the kinematic viscosity.

The relative uncertainty of the thermal resistance is expressed as [11]

$$\frac{\delta R_{\text{th}}}{R_{\text{th}}} = \left\{ \left[\frac{\delta(T_{\text{ave}} - T_{\infty})}{T_{\text{ave}} - T_{\infty}} \right]^2 + \left(\frac{\delta Q}{Q} \right)^2 \right\}^{1/2} \tag{4}$$

The relative uncertainties of the heating power Q and the impinging Reynolds number Re are obtainable in similar ways. The relative uncertainties of the thermal resistance, the heating power, and the Reynolds number for the experiments are estimated to be 11.9%, 4.9%, and 2%, respectively.

3. Results and discussion

In heat sink applications, there are many important parameters that can be modified to enhance the thermal performance. As experimental parameters we investigate the influence of the Reynolds number Re, the width W and the height H of the fins, the type of the heat sinks, and the distance Y from the nozzle to the tip of the fins on the thermal resistance.

3.1. Temperature distribution on the surface of the heat sink

Fig. 4 depicts the infrared thermal image of the top surface of the heat sink by infrared thermography under the conditions $Y/D = 12$, $W/L = 0.08125$, $H/L = 0.5625$, $Q = 20.31$ W, $Re = 20{,}000$. The temperature gradient indicates the direction of heat transfer in the heat sink to be outward from the inside and upward from the bottom.

3.2. Influence of the impinging jet on the thermal performance of pin–fin heat sinks

The thermal resistance of the pin–fin heat sinks with various widths and heights with a jet impinging at $Y/D = 12$ and $Re = 5000$–$20{,}000$ is shown in Fig. 5. The thermal resistance decreases with increasing fin width and Reynolds number. The effects of the fin width on the thermal resistance are obvious, especially at $Re = 5000$. The differences of the thermal resistance with varied height become diminished as the Reynolds number increases. It is noted that increasing the Reynolds number reduces the thermal resistance consistently. Moreover, the reduction of the thermal resistance decreases with the increase of the Reynolds number. The curves of the thermal resistances at $Re = 25{,}000$ almost coincide with those for $Re = 20{,}000$, which are omitted for clarity of the figure. It is also noted that the thermal resistance is rather independent of the height of the fins and depends only on the width for a Reynolds number greater than 15,000.

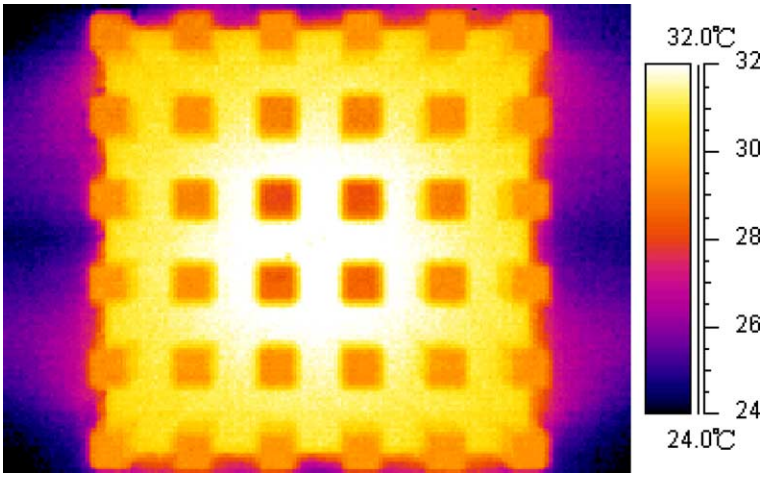

Fig. 4. The temperature distribution of a pin–fin heat sink under the conditions $Y/D = 12$, $W/L = 0.08125$, $H/L = 0.5625$, $Q = 20.13$ W, $Re = 20{,}000$.

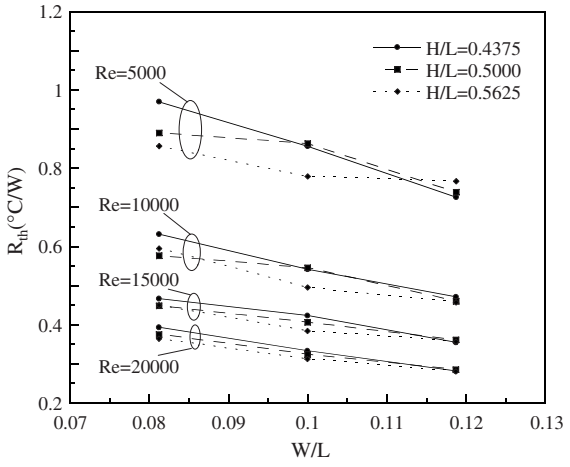

Fig. 5. The influence of the impinging Reynolds number and the fin dimensions on the thermal resistance of pin–fin heat sinks with $Y/D = 12$.

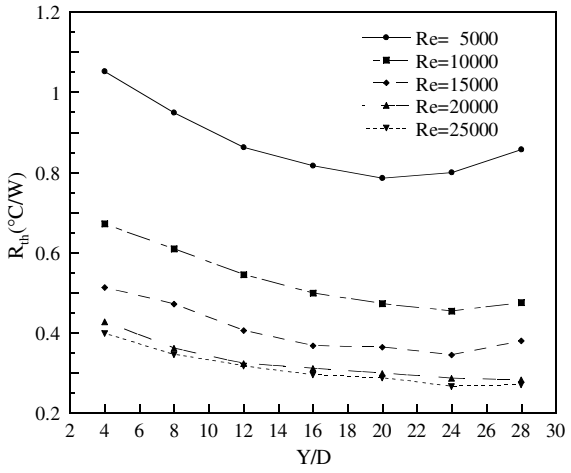

Fig. 6. The influence of the impinging distance on the thermal resistance of a pin–fin heat sink with $W/L = 0.1$ and $H/L = 0.5$.

3.3. Influence of the impinging distance on the thermal performance of pin–fin heat sinks

Fig. 6 shows the influence of the distance from the nozzle to the tip of the heat sink and the impinging Reynolds number on the thermal resistance of a pin–fin heat sink with geometry $W/L = 0.1$ and $H/L = 0.5$. The thermal resistance increases when the distance is too small. An appropriate distance with $Y/D = 20$ is found to yield a minimum thermal resistance at $Re = 5000$. Further increasing the impinging distance results in a lack of fluid momentum to drive effective force convection, thus the thermal resistance increases. The appropriate distance increases with increasing Reynolds number of the impinging jet. Moreover, the improvement of the thermal resistance by increasing the impinging distance for higher Reynolds numbers is not as significant as that for $Re = 5000$.

Fig. 7 depicts the behaviors of three heights, i.e. $H/L = 0.4375$, 0.5 and 0.5625, of the pin–fin heat sinks at various Reynolds numbers with a constant width ratio $W/L = 0.1$ and two impinging distance ratios $Y/D = 8$ and 12. Eq. (2) reveals that the thermal resistance can be reduced by increasing the product of the overall heat transfer coefficient and the heat transfer area. The optimal thermal performance in the figure occurs at $Y/D = 12$ and $H/L = 0.5625$, and there is little variation for a Reynolds number greater than 20,000 with $Y/D = 12$, although the influence of the Reynolds

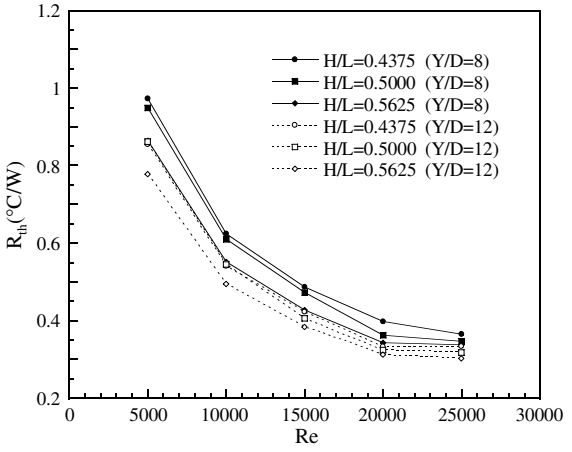

Fig. 7. The influence of the fin height on the thermal resistance at various Reynolds numbers with $W/L = 0.1$ and two impinging distance ratios $Y/D = 8$ and 12.

number is still obvious for a small distance ratio $Y/D = 8$ of the impinging jet with a height ratio $H/L = 0.4375$ of the fins from comparison with $Y/D = 12$. The curves for both $H/L = 0.4375$ with $Y/D = 12$ and $H/L = 0.5625$ with $Y/D = 8$ nearly coincide in the figure; hence the effect of a small impinging distance becomes improved on increasing the height of fins.

Fig. 8 shows the influence of the width of fins on the thermal resistance at various Reynolds numbers with a constant height ratio $H/L = 0.5$ and two impinging distance ratios $Y/D = 8$ and 12. The case with $Y/D = 12$ and $W/L = 0.11875$ has superior thermal performance. The width of fins plays a more important role on the thermal performance improvement with increasing distance of the impinging jet. The more distinct behavior at greater impinging distance ratio $Y/D = 12$ might reflect that local heat transfer is dominated by the exposure surface with decreasing penetrating momentum, whereas the behavior at small impinging distance ratio $Y/D = 8$ might reflect that the local heat transfer is dominated by the penetrating momentum and the influence of the exposure surface on the thermal resistance is less significant.

3.4. Comparison of thermal performance between pin–fin heat sinks and plate–fin heat sinks

The comparison of the thermal resistance between pin–fin heat sinks and plate–fin heat sinks at various width ratios W/L and Reynolds numbers Re with $Y/D = 12$ and $H/L = 0.5$ is shown in Fig. 9. According to Table 1 the total exposure surface of the plate–fin heat sink is greater than that of the pin–fin heat sink for the case $W/L = 0.08125$. In contrast, the total exposure surface of the pin–fin heat sink is greater than that of the plate–fin heat sink for the case $W/L = 0.1$ and 0.11875. The pin–fin heat sink with the width ratio $W/L = 0.11875$ shows the least thermal resistance. The exposure surface of the plate–fin heat sink with $W/L = 0.08125$ is greater than that of the pin–fin heat sink. However, in the plate–fin heat sink flow resistance restricts its convective ability and results in a higher thermal resistance as $Re < 15{,}000$. The situation becomes different for $Re = 20{,}000$ and 25,000 as the penetrating momentum is sufficient to overcome the flow resistance and the greater exposure surface of the plate–fin heat sink with $W/L = 0.08125$ produces a smaller thermal resistance than the pin–fin heat sink. As the width ratio W/L becomes equal to 0.1, the thermal resistances of the

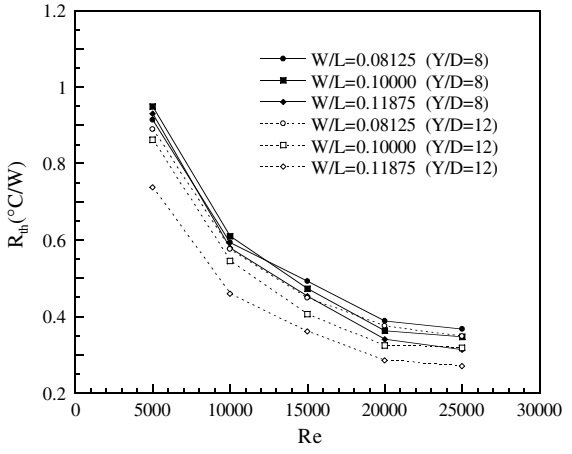

Fig. 8. The influence of the fin width on the thermal resistance at various Reynolds numbers with $H/L = 0.5$ and two impinging distance ratios $Y/D = 8$ and 12.

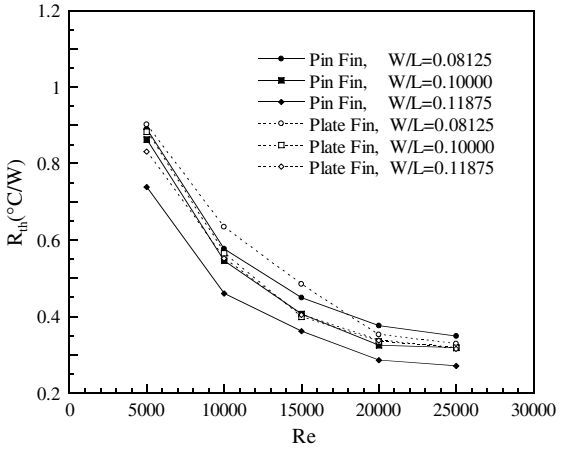

Fig. 9. The comparison of the thermal resistance between pin–fin heat sinks and plate–fin heat sinks at various fin widths and Reynolds numbers with $Y/D = 12$ and $H/L = 0.5$.

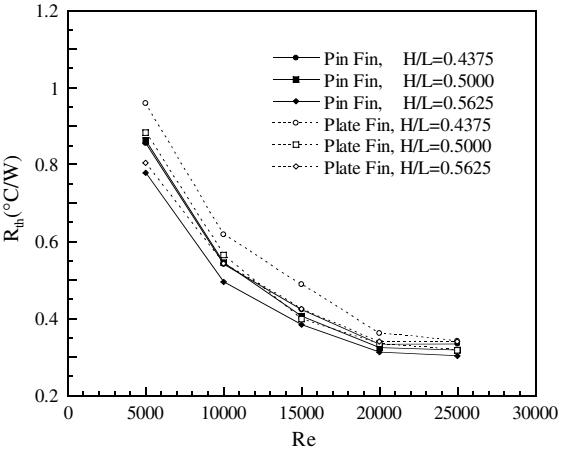

Fig. 10. The comparison of the thermal resistance between pin–fin heat sinks and plate–fin heat sinks at various fin heights and Reynolds numbers with $Y/D = 12$ and $W/L = 0.1$.

two types of heat sinks are similar. Hence the pin–fin heat sink of smaller volume but greater exposure surface is preferable because of its smaller cost.

Fig. 10 shows the comparison of the thermal resistance between pin–fin heat sinks and plate–fin heat sinks at various heights of fins and Reynolds numbers with $Y/D = 12$ and $W/L = 0.1$. With the height ratio $H/L = 0.4375$, the pin–fin heat sink has a greater exposure surface than the plate–fin heat sink. The pin–fin heat sink exhibits a smaller thermal resistance over the entire range of Reynolds number. The deviations of the thermal resistance between the pin–fin heat sinks and the plate–fin heat sinks at $Re < 15{,}000$ are greater than at $Re > 15{,}000$. The thermal resistances of both pin–fin heat sinks and plate–fin heat sinks exhibit almost the same values with the height ratio $H/L = 0.5$ of the fins, whereas the deviation of the exposure surface is greater than that for $H/L = 0.4375$. Hence for ratios $W/L = 0.1$ and $H/L = 0.5$ of geometric parameters at $Y/D = 12$, the cheaper heat sink of these types can be chosen without loss of cooling performance. As the height ratio increases to $H/L = 0.5625$, the pin–fin heat sink shows 0.3–0.5 °C/W less thermal resistance than the plate–fin heat sink.

4. Conclusions

We have investigated the effects of the width and height of the fins and the distance from the nozzle to the tip of the fins at various Reynolds numbers on the thermal performance of the heat sinks with confined impingement cooling through the use of infrared thermography. We conclude as follows from the experimental results.

1. The Reynolds number of the impinging jet plays an important role in the thermal resistance. Increasing the Reynolds number consistently diminishes the thermal resistance. The slope of the decrease also lessens with increasing Reynolds number.
2. Increasing the width of the fins increases the total exposure surface of the heat sink, which basically enhances heat convection. With the constrained of fixed dimensions of the heat sink base, increasing the width of the fins implies that interfin flow passages decrease, consequently increasing the flow resistance. Therefore increasing the width of the fins combined with an appropriate Reynolds number can improve the thermal performance.
3. Increasing the height of the fins results in increased total exposure surface of the heat sink, which also enhances the thermal performance, but the height of the fins beyond a critical value might also impede the penetrating ability of the impinging jets. When that condition occurs, it can be overcome by increasing the Reynolds number of the impinging jet. The thermal resistance is decreased more effectively by increasing the width of the fins than by increasing the height of the fins.
4. The influences of geometric dimensions on the thermal performance are more pronounced at small Reynolds number than at large Reynolds number. For a small Reynolds number, a feasible match of dimensions of the fins is crucial.
5. There is an appropriate impinging distance which corresponds to a minimum thermal resistance at a specific Reynolds number. The distances of the minimum thermal resistance increase with increasing Reynolds number. Moreover, the improvement of the thermal resistance by increasing the impinging distance is more significant for a small Reynolds number.

Acknowledgement

The support of this work by the National Science Council of the Republic of China under contract no. NSC 93-2212-E-211-004 is gratefully acknowledged.

References

[1] E. Yu, Y. Joshi, Heat transfer enhancement from enclosed discrete components using pin–fin heat sinks, Int. J. Heat Mass Transfer 45 (2002) 4957–4966.

[2] S. Sathe, K.M. Kelkar, K.C. Karki, C. Tai, C. Lamb, S.V. Patankar, Numerical prediction of flow and heat transfer in an impingement heat sink, J. Electron. Packaging 119 (1997) 58–63.

[3] K.L. Teuscher, S. Ramadhyani, F.P. Incropera, Jet impingement cooling of an array of discrete heat sources with extended surfaces, enhanced cooling techniques for electronics applications, ASME HTD 263 (1993) 1–10.
[4] L.A. Brignoni, S.V. Garimella, Experimental optimization of confined air jet impingement on a pin fin heat sink, IEEE Trans. Components Packaging Technol. 22 (1999) 399–404.
[5] G. Ledezma, A.M. Morega, A. Bejan, Optimal spacing between pin fins with impinging flow, J. Heat Transfer 118 (1996) 570–577.
[6] J.G. Maveety, H.H. Jung, Design of an optimal pin–fin heat sink with air impingement cooling, Int. Comm. Heat Mass Transfer 27 (2000) 229–240.
[7] E.R. Meinders, T.H. vander Meer, K. Hanjalić, C.J.M. Lasance, Application of infrared thermography to the evaluation of local convective heat transfer on arrays of cubical protrusions, Int. J. Heat Fluid Flow 18 (1997) 152–159.
[8] E.R. Meinders, K. Hanjalić, Vortex structure and heat transfer in turbulent flow over a wall-mounted matrix of cubes, Int. J. Heat Fluid Flow 20 (1999) 255–267.
[9] H. Ay, J.Y. Jang, J.N. Yeh, Local heat transfer measurements of plate finned-tube heat exchangers by infrared thermography, Int. J. Heat Mass Transfer 45 (2002) 4069–4078.
[10] H.Y. Li, K.Y. Chen, Thermal-fluid characteristics of pin–fin heat sinks cooled by impinging jet, J. Enhanced Heat Transfer 12 (2005) 189–201.
[11] R.J. Moffat, Using uncertainty analysis in the planning of an experiment, J. Fluids Eng. 107 (1985) 173–179.